Impact-parameter dependence of energy loss for 625-keV H^+ ions in Si single crystals

A. Dygo,* M. A. Boshart, and L. E. Seiberling

Department of Physics, University of Florida, P.O. Box 118440, Gainesville, Florida 32611-8440

N. M. Kabachnik

Institute of Nuclear Physics, Moscow State University, 119899 Moscow, Russia
(Received 19 July 1994)

The energy distributions for 625-keV H^+ ions transmitted through thin Si single crystals are studied for detailed angular scans through the $\langle 110 \rangle$ and $\langle 100 \rangle$ axial as well as the $\{111\}$ and $\{110\}$ planar channels. Well-resolved structures in the distributions taken near the $\langle 110 \rangle$ axial direction are observed. The experimental energy-loss distributions are very well reproduced by a Monte Carlo simulation using the semiclassical approximation model for core electrons and the two-component free-electron-gas model for valence electrons. The best fit to the data is obtained if the model energy losses are scaled up for core electrons and down for valence electrons by several percent. The experimental distributions can also be reproduced by assuming the mean excitation energy for distant collisions of the ion with core electrons equal to 1.4 times the binding energy for a given shell. No significant differences between the distributions obtained using the solid-state and free-atom valence electron densities have been found. The evolution of the distributions for the $\langle 110 \rangle$ axial scan is discussed in terms of ion trajectories and the flux distribution. Also, the azimuthally averaged mean energy loss is studied as a function of tilt angle with respect to the $\langle 110 \rangle$ axis.

PACS number(s): 61.80.Mk, 61.80.Jh, 79.20.Nc, 79.20.Rf

I. INTRODUCTION

The stopping of energetic ions in crystalline materials is known to strongly depend on the direction of incidence. In particular, ions moving along a major crystallographic axis lose their energy at a rate that can be as low as 50% or less of the so-called normal or random value. This reduced stopping is one of the dominant features of the channeling phenomenon [1]. The random stopping, on the other hand, occurs for directions far from any significant axial or planar channels, where the crystal lattice appears to the ion beam as a randomlike arrangement of atoms. The reduced stopping of channeled ions is easily understood in terms of the impact-parameter dependence of the energy loss that occurs in a single ion-atom collision. The channeled ions maintain large distances from the atom rows and therefore can only make small energy transfers to the atomic cores. Similarly, the contribution of valence (outer-shell) electrons to the stopping is diminished, as their density in the central region of the channel is reduced.

An understanding of H ion stopping is essential for studies of a broad range of stopping phenomena and a good deal of effort has been expended to explore the orientation effects in the stopping of H ions in crystals (see Refs. [1–4] for surveys of the pre-1982 work). The experimental studies published so far have concentrated

mainly on the reduced stopping for ions transmitted through thin single crystals along major axial and planar channels [5–12]. In addition, following the 1965 seminal article on channeling by Lindhard [13], a large number of theoretical studies on the impact-parameter-dependent energy loss $\Delta E(b)$ have appeared [14–31].

The principal quantity of interest extracted from the observed energy distributions has been the leading edge value, corresponding to the energy loss of the best channeled ions. Thus comparisons between experiment and theory have usually been restricted to the energy loss corresponding to impact parameters close to the channel radius (axial channeling) or the channel half-width (planar channeling). Such comparisons are often ambiguous due to the inability to resolve various contributions to the energy loss [19]. Further, an extraction of the leading edge value from experimental distributions is subject to uncertainties related to energy straggling and energy resolution factors [32]. The situation is much improved if full energy-loss distributions are utilized, allowing comparisons between experiment and theory over a broader range of impact parameters. Such an approach, however, requires modeling of individual particle trajectories in the crystal by the Monte Carlo technique and only a few attempts to simulate full energy distributions have been published so far [32–38].

In the present paper, energy-loss distributions for 625-keV H^+ ions in thin Si single crystals are studied as a function of the crystal orientation. Detailed angular scans are taken through the $\langle 110 \rangle$ and $\langle 100 \rangle$ axes as well as through the most open planar channels intersecting these axial directions, i.e., the $\{111\}$ and $\{110\}$ planes, respectively. The experimental distributions are

*Permanent address: Soltan Institute for Nuclear Studies, Warsaw, Poland.

very well reproduced by a Monte Carlo simulation using the semiclassical approximation (SCA) of Kabachnik, Kondratev, and Chumanova [28] to describe the energy loss to core electrons and the free-electron-gas (FEG) model to determine the energy loss to valence electrons. It is found that the mean excitation energy approximation, used to calculate the impact-parameter dependence of the core electron contribution to the stopping in our preliminary report [39], can reproduce the SCA results quite well. Various approaches to the valence electron contribution are also analyzed: the Lindhard-Winther local-density approximation [40] versus the constant density approximation, as well as the use of the solid-state versus free-atom electron densities. Based on individual ion trajectories and ion flux distribution calculations, the evolution of the energy distributions as a function of tilt angle with respect to the axial direction is discussed. Also, randomlike directions near the $\langle 110 \rangle$ axis are identified by means of a detailed study of the orientation dependence of the mean energy loss.

II. EXPERIMENT

Two separate experiments were performed to measure the energy distributions for directions near the $\langle 110 \rangle$ and $\langle 100 \rangle$ axes, using two different Si single crystals. As the equipment and procedures used in the two experiments were essentially the same and the $\langle 100 \rangle$ experiment is described in our earlier communication [39], we will confine ourselves in this section to the $\langle 110 \rangle$ experiment.

The incident beam of H^+ ions, produced and accelerated to 625 keV by the University of Florida 3.5-MV Van de Graaff accelerator, was collimated to a cross-sectional area of 0.8×0.8 mm^2 and an angular divergence of $0.03°$. A 1.2-μm-thick Si(110) sample was prepared using a dopant-selective etching technique [41] and a 10-Å-thick amorphous layer of Au was deposited on the 10% HF-dipped surface. The etched area of the sample had a diameter of 5 mm, with a thickness variation of 5–10 %. The sample was mounted on a two-axis goniometer, stepper motor driven with a resolution of $0.02°$. The goniometer was also equipped with translation perpendicular to the beam. The ions scattered through $80°$ were detected in a transmission geometry (the Au layer on the beam exit side, as shown in Fig. 1) and energy analyzed using a Si surface-barrier detector with an acceptance angle of $2.5°$. The base pressure in the scattering chamber was 5×10^{-6} Torr.

The scattering yield from Si was used to align planar and axial directions to the beam. The goniometer-beam system was calibrated and the alignment for any direction in the crystal was achieved to a precision of $0.02°$–$0.05°$ by applying the methodology developed in Ref. [42]. Both the multichannel analyzer and the stepper motors on the goniometer were controlled by a personal computer. Once reference directions were established (usually an axial and a planar direction), the energy distributions corresponding to full angular scans in the crystal coordinates, involving rotations about both axes of the goniometer, were taken in a completely automated way.

The energy distributions of the H ions transmitted through the Si single crystal were retrieved from the Au signal by dividing the measured energy by the kinematic factor. A total of 21 distributions were taken on the same target spot to ensure no variation in sample thickness. Each distribution was collected for 0.8 μC of the integrated beam charge. Two angular scans were performed: (i) through the $\langle 110 \rangle$ axis along the $\{111\}$ plane and (ii) perpendicular to the $\{111\}$ plane at a tilt $\theta = 10°$ with respect to the $\langle 110 \rangle$ axis. The tilts included in scan (i) were $\theta = 0°$ (i.e., the $\langle 110 \rangle$ axis), $0.2°$, $0.4°$, $0.6°$, $0.8°$, $1°$, and $2°$, while the azimuthal angles studied in scan (ii) were $\phi = 0°$ (i.e., the $\{111\}$ plane), $0.5°$, $1°$, $1.5°$, $2.5°$, $5°$, and $10°$ ($\phi = 54.74°$ corresponds to the $\{100\}$ plane, while $\phi = -35.26°$ corresponds to the $\{110\}$ plane). Based on our simulation results presented in Sec. IV C, the tilt of $10°$ is large enough to avoid the influence of the $\langle 110 \rangle$ axis. The direction $(\theta, \phi) = (10°, 0°)$ can thus be considered to represent a "pure" $\{111\}$ plane. It will be further shown that the mean energy loss for the direction $(\theta, \phi) = (10°, 10°)$ approximates the random value to better than 1%.

As a consistency check, a number of randomlike distributions (for specific directions) were taken, followed by a repeated measurement of the $\langle 110 \rangle$ distribution. Comparison between the two measurements for the $\langle 110 \rangle$ direction revealed a slight change in the shape of the distribution as well as a shift toward lower energies. These changes are primarily due to carbon deposition on both sides of the sample during the irradiation. Changes in the distribution can also result from structural defects in the sample, introduced by the irradiation. However, as the distributions for the most sensitive directions (close to the $\langle 110 \rangle$ axis) were taken at the beginning of the measurement sequence, they do not seem likely to be affected by significant radiation damage. In order to determine the amount of the shift due to the carbon layers, the distributions for the direction $(\theta, \phi) = (10°, 10°)$ were taken at the beginning of each scan [in addition to the measurement at the end of scan (ii)], as well as at the end of the whole sequence. The magnitude of the shift for all other distributions was determined by linear interpolation based on the accumulated beam dose and the distributions were corrected accordingly. The estimated shift corresponded to about 10^{16} C atoms/(cm$^2 \mu$C) deposited on both sides of the sample.

The sample thickness, the normalization constant for all distributions, as well as overall energy resolution are determined based on the distribution for the direction $(\theta, \phi) = (10°, 10°)$ by requiring that the simulated distribution (see Sec. III) matches the experiment. The distributions for randomlike directions depend on the random value of the stopping cross section assumed in the simulation, but are insensitive to the impact-parameter dependence of the energy loss. As the random stopping cross section is known in our energy range to an accuracy better than 5%, the same (in)accuracy is achieved in the thickness determination. This does not affect the energy distributions because for a sample about 1 μm thick, the ion flux distribution (and, consequently, the energy distribution if normalized to the random energy loss) does not change significantly if the thickness is increased (de-
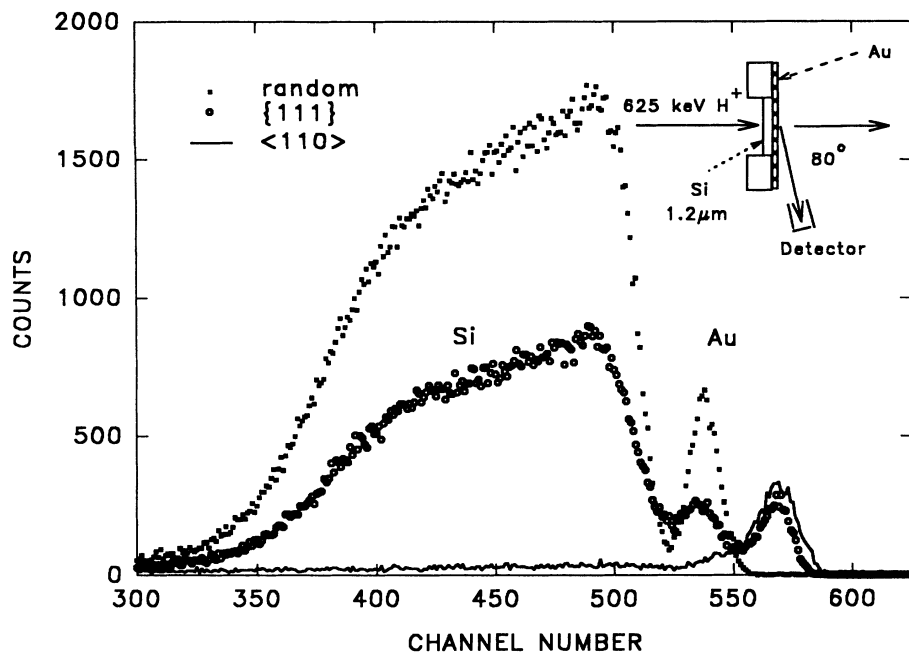
FIG. 1. Energy spectra for 625-keV H ions transmitted through 1.2-μm-thick Si crystal and scattered through 80°, taken in the random, aligned with the {111} planar and ⟨110⟩ axial directions.

creased) by 5%. The overall energy resolution was found to be 10 keV. This value includes the detection system resolution, the energy spread of the incident beam, and the effect of the sample nonuniformity.

A final note concerns the overlap of the Si and Au signals seen in Fig. 1. The Si signal consists, in fact, of two components: one that is due to scattering within the single-crystalline material and the other one coming from scattering by the amorphous oxide layer at the Au/Si interface. The latter registers the energy distribution of the transmitted ions in the same way as the Au signal does. However, it appears shifted to lower energies and is much weaker than the Au signal, due to the smaller kinematic factor and scattering cross section of Si, as well as the smaller thickness of the oxide. It can be estimated that the shift amounts to 29 keV for the ⟨110⟩ direction and 27 keV for the random direction (cf. the energy distributions presented in Sec. IV A).

III. ENERGY DISTRIBUTION CALCULATIONS

The main purpose of this work is to investigate the energy loss suffered by H ions in individual collisions with Si atoms over a wide range of impact parameters. In order to utilize all the information available in experiment, full energy distributions for detailed scans through channeling directions will be considered. Calculations of such distributions can be best done by means of a Monte Carlo simulation. In Sec. III A, details of the simulation code used will be presented, while the energy-loss models examined will be described in Sec. III B.

A. Monte Carlo simulation of ion trajectories

In a Monte Carlo simulation, one follows a large number of ion trajectories in the crystal, taking all the interactions involved into account as closely as possible.

These include scattering of the ion by the screened Coulomb field of the crystal atoms, multiple scattering by electrons, energy loss processes, effects of surface layers and the incident beam angular divergence, as well as thermal vibrations of the crystal atoms. The CXX simulation code, originally described in Refs. [34] and [43] and subsequently updated in Ref. [44], was used in this work. The code has been successfully tested against backscattering experiments in Si and $A^{III}B^{V}$ single crystals [43–48]. The backscattering energy spectra show high sensitivity to details of ion trajectories, but are rather insensitive to the position dependence of the ion stopping power. Thus, in the present calculations we retain most of the simulation parameters as determined from these experiments. The major modifications to the "backscattering" version of the code pertain to the energy-loss calculations, as presented in Sec. III B.

In calculating the energy distributions discussed in Sec. IV A, the H-Si interaction potential [46,47], based on the Hartree-Fock electronic density modified to account for solid-state effects [49], and the vibrational amplitude of 0.078 Å were used. The incident beam angular divergence of 0.03° (standard deviation), corresponding to the experimental conditions, was taken into account. The calculations of the angular spread due to thin amorphous surface layers were done in a Monte Carlo fashion by evaluating individual ion-atom collisions (using the Ziegler-Biersack-Littmark universal potential [49] for atoms other than Si). Typically, 3200–6400 ion trajectories were followed to generate a single energy distribution. Energy straggling was not included within the simulation code, but separately, by convolving simulated distributions (channel by channel) with a Gaussian distribution of the appropriate standard deviation dependent on the energy loss. The amount of straggling was determined based on Ref. [50] by converting the dependence of straggling on the penetration depth into a dependence

on energy loss (assuming random stopping power). Due to widely differing energy losses from channeled to random distributions, the energy dependence of the H-Au cross section was taken into account. Finally, small changes in the path length for ions penetrating the crystal along different directions were considered in the simulations.

B. Energy-loss models

We make the usual assumption that core and valence electrons contribute independently to the stopping. The interaction of the ion with valence electrons is treated within the (FEG) theory. The energy losses to valence electrons are divided into the contribution due to single-particle excitations that occur in close collisions and the contribution due to collective (plasma) excitations that occur via distant collisions. The first contribution is assumed to be proportional to the local valence electron density, while the second one is taken proportional to the average valence electron density. The energy lost by the ion (to core and valence electrons) in an individual collision with the lattice atom, for an impact parameter b, can thus be written as

$$\Delta E_a(b) = \Delta E_c(b) + \Delta E_{v1}(b) , \tag{1}$$

where ΔE_c represents the energy loss to core electrons and ΔE_{v1} is the energy lost in close collisions with valence electrons of the atom. The energy loss due to collective excitations of the valence electron gas, not being associated with any particular ion-atom collision, does not enter into Eq. (1).

When the impact-parameter-dependent energy loss is integrated over all b's, one gets the respective stopping cross section, for instance,

$$\varepsilon_c = \int_0^\infty \Delta E_c(b) 2\pi b \, db . \tag{2}$$

Similarly, ε_{v1} and $\varepsilon_a = \varepsilon_c + \varepsilon_{v1}$ are obtained by integrating ΔE_{v1} and ΔE_a, respectively. It is convenient to normalize the above energy losses by their corresponding stopping cross sections, which defines functions of b referred to as $L(b)$. For example,

$$L_c(b) = \frac{\Delta E_c(b)}{\varepsilon_c} . \tag{3}$$

Within the restricted energy interval considered here, the dependence of the functions L on the energy (velocity) of the ion can be neglected. Obviously, they satisfy the normalization condition

$$\int_0^\infty L(b) 2\pi b \, db = 1 . \tag{4}$$

The total (random) stopping cross section is given by

$$\varepsilon_r = \varepsilon_a + \varepsilon_{v2} = \varepsilon_c + \varepsilon_{v1} + \varepsilon_{v2} , \tag{5}$$

where ε_{v2} is the contribution due to distant collisions with the valence electron gas (plasmon excitation). In the calculations to be presented in Sec. IV, ε_r is taken from the semiempirical tables of Ref. [51].

1. Core electrons: The semiclassical approximation

The energy loss due to core electrons is calculated within first-order perturbation theory using the SCA method of Kabachnik, Kondratev, and Chumanova [28]. The method involves an explicit summation of all contributions due to excitation and ionization of the atom which is described by the Hartree-Slater approximation. The SCA model was successfully applied to explain data on the angular dependence of the energy loss in thin films [52]. In contrast to channeling experiments, these data are most sensitive to small impact parameters. The model was also used in a number of studies on energy loss of channeled protons and antiprotons [53,36]. Recently, good agreement with the SCA model predictions was found by Auth and Winter in a study of the energy loss of 100-keV protons in single collisions with Ar atoms [54]. Additionally, the calculation of the impact-parameter-dependent straggling within SCA agreed very well with experimental data [55].

The L_c function for a 625-keV H ion on a Si core, calculated within the SCA model, is plotted in Fig. 2. In this calculation, the energy loss due to excitation to bound states is neglected, as it is estimated to contribute about 5% to the total energy loss. The calculation indicates that K-shell electrons give a significant contribution to the energy loss at very small impact parameters only (about 16% for $b = 0$ and rapidly vanishing by $b = 0.1$ Å). One can conclude, therefore, that the K-shell electron contribution to the stopping cross section is negligible [cf. Eq. (2)].

2. Core electrons: The mean excitation energy approximation

As an alternative approach, we divide the core electron contribution to the stopping (ε_c) into the close collision part (ε_{c1}) and the distant collision part (ε_{c2}). Assuming the equipartition rule [40] we have $\varepsilon_{c1} = \varepsilon_{c2}$. The
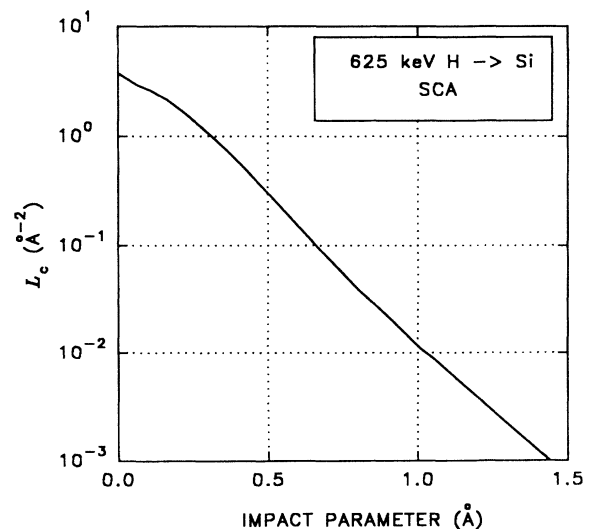
FIG. 2. L_c function for 625-keV H ion on a Si core calculated within the SCA model.

position-dependent stopping cross section related to close collisions is assumed to be proportional to the local density of core electrons, while the energy loss due to distant collisions is calculated within the dipole approximation with the mean excitation energy (cf. the four-component model in Ref. [39]). Hence the energy loss due to close collisions with core electrons is given by $\Delta E_{c1} = \varepsilon_{c1} L_{c1}(b)$, where

$$L_{c1}(b) = \frac{1}{Z_c} \int_{-\infty}^{+\infty} n_c(\mathbf{r}) dz \ . \tag{6}$$

Z_c denotes the number of core electrons per atom and $n_c(\mathbf{r})$ is the core electron density (associated with a single atom). The integral is taken along the ion's trajectory (as it passes the atom), which is approximated by a straight line ($r^2 = b^2 + z^2$). Based on the SCA calculations, the contribution of K-shell electrons to the stopping of 625-keV H ions can be neglected (cf. Sec. III B 1). Therefore, only L-shell electrons are included when evaluating Eq. (6). Their density is determined based on the Roothaan-Hartree-Fock (RHF) atomic wave functions [56].

To calculate the distant collision term L_{c2}, the dipole approximation as discussed by Kumakhov and co-workers [19,4] is used. Assuming a mean electronic excitation energy $\hbar\omega_j$ for a shell j, the energy transferred to a single electron l can be written as

$$\Delta E_{lj}(b) = \frac{2Z_1^2 e^4}{m_e v^2 b_j^2} \Omega_j^2 \left[K_0^2 \left[\Omega_j \frac{b}{b_j} \right] + K_1^2 \left[\Omega_j \frac{b}{b_j} \right] \right] , \tag{7}$$

where Z_1 is the projectile atomic number, e is the electron charge, m_e is the electron mass, v is the projectile velocity, $\Omega_j = \omega_j / \omega_{j\infty}$ is the mean excitation energy ($\hbar\omega_j$) measured relative to the binding energy ($\hbar\omega_{j\infty}$), $b_j = v / \omega_{j\infty}$, and K_0 and K_1 are the modified Bessel functions. Again, Eq. (7) is applied to the L I, L II, and L III shells only. (Their respective binding energies are 149.7, 99.8, and 99.2 eV [57].) By summing over all electrons in inner shells, one thus gets $\Delta E_{c2}(b) = \sum_j \sum_l \Delta E_{lj}(b)$ and $L_{c2}(b) = \Delta E_{c2}(b)/\varepsilon_{c2}$. However, Eq. (7) is derived for impact parameters greater than the shell radius and it diverges for $b \to 0$. In order to evaluate L_{c2} for small b, a third-order polynomial form was assumed: $L_{c2}(b) = c_0 + c_1 b + c_2 b^2 + c_3 b^3$. The cutoff value of the impact parameter b_c, where the two branches meet, and the parameters c_i ($i = 0, \ldots, 3$) were uniquely determined by requiring that (i) the derivative of L_{c2} at $b = 0$ vanishes, (ii) both the L_{c2} and its derivative at $b = b_c$ for the two branches are equal to each other, (iii) Eq. (4) is fulfilled, and (iv) L_{c2} monotonically decreases between 0 and b_c and the difference between $L_{c2}(0)$ and $L_{c2}(b_c)$ is as small as possible. For example, if one assumes $\Omega_j = 1$, the resulting b_c (for 625-keV H on Si) is 0.64 Å, while for $\Omega_j = 1.4$ one gets $b_c = 0.46$ Å.

The L_c functions (i.e., $\frac{1}{2}L_{c1} + \frac{1}{2}L_{c2}$), calculated within the mean excitation energy approximation (MEEA) for three values of the parameter Ω (1, 1.2, and 1.4), are compared with the SCA dependence in Fig. 3. While $\Omega = 1$
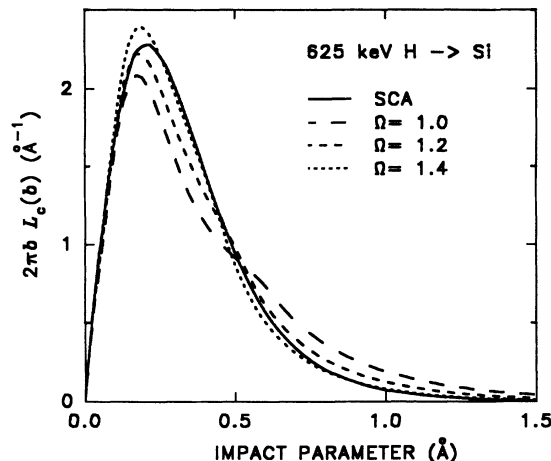
FIG. 3. $2\pi b L_c$ functions calculated within the MEEA model for three values of Ω (and $\beta = 0.94$), compared with the SCA calculation.

clearly overestimates the energy loss for large impact parameters ($b > 0.5$ Å), the curve for $\Omega = 1.4$ is remarkably close to the SCA prediction in the whole range of impact parameters [58]. Let us note that within the MEEA model, $\Delta E_{c2}(b)$ (for $b > b_c$) and ε_{c2} are independent of each other, so the resulting L_{c2} function depends on the chosen value of ε_{c2}. The latter, in turn, is related to ε_v ($= \varepsilon_{v1} + \varepsilon_{v2}$) through the equation $\varepsilon_{c2} = \frac{1}{2}(\varepsilon_r - \varepsilon_v)$, where the random stopping cross section ε_r is a fixed quantity (for a given energy). The value of ε_v is determined by the parameter β, defined in Sec. III B 3 . The results presented in Fig. 3 were calculated for $\beta = 0.94$. This value corresponds to the best fit to the experimental energy distributions, obtained using the SCA model (see Sec. IV A).

3. Valence electrons

As mentioned earlier, the valence electron contribution to the stopping is treated within the free-electron-gas theory. The stopping cross sections due to close and distant collisions are calculated according to the formulas [6]

$$\varepsilon_{v1} = \beta \frac{4\pi Z_1^2 e^4}{m_e v^2} Z_v \ln \frac{2 m_e v v_F}{\hbar \omega_p} \tag{8}$$

and

$$\varepsilon_{v2} = \beta \frac{4\pi Z_1^2 e^4}{m_e v^2} Z_v \ln \frac{v}{v_F} , \tag{9}$$

where Z_v is the number of valence electrons per atom and β is introduced here as a scaling parameter. In the above formulas the Fermi velocity v_F and the plasmon energy $\hbar\omega_p$ are calculated for the average density of valence electrons in the crystal.

Based on the assumption that the position-dependent stopping due to close collisions is proportional to the lo-

cal density of valence electrons, one gets the formula for L_{v1} that is analogous to Eq. (6) for the core electron term L_{c1}. However, the valence electron density (associated with a given atom) extends to much larger distances than the core electron density does. More importantly, due to the directional bonding effects, the valence electron density in solid Si is not isotropic. Thus, in general, the L_{v1} function depends on the impact parameter vector **b** rather than on its absolute value b. Therefore, from a programming point of view, it is convenient to calculate a two-dimensional map $L_{v1}(\mathbf{b})$ across the channel, to be used in the simulation code. The $L_{v1}(\mathbf{b})$ map is no longer associated with a single atom, but includes contributions from all atoms that are sufficiently close to a given point within the channel area. Consequently, the argument **b** ceases to be an impact parameter with respect to any particular atom. Instead, it is a two-dimensional position vector with respect to a chosen frame of reference. The use of $L_{v1}(\mathbf{b})$ map simplifies and speeds up the simulations, but it is strictly valid only for trajectories parallel to the axis along which the electron density is integrated. For trajectories tilted by ψ with respect to the axis, the energy loss is approximated by $\varepsilon_{v1}L_{v1}(\mathbf{b})/\cos\psi$.

Maps of $L_{v1}(\mathbf{b})$ were tabulated for both solid-state and free-atom valence electron densities with a resolution of 0.0543 Å (along the $\{110\}$ plane)$\times$0.0384 Å (along the $\{100\}$ plane) for the $\langle 110 \rangle$ axis and a resolution of 0.0384×0.0384 Å^2 (along the $\{110\}$ planes) for the $\langle 100 \rangle$ axis. The solid-state electron density was taken from the analysis of x-ray diffraction measurements by Deutsch [59], while the free-atom electron density was based on the RHF wave functions [56]. Both maps consider contributions to the density from all atoms (on a given atomic plane) within a distance of about 4 Å.

The L_{v1} functions corresponding to the solid-state and free-atom valence electron densities are compared in Figs. 4 and 5. In order to reflect the symmetry of the channel, the values plotted include contributions of two successive planes for the $\langle 110 \rangle$ axis and four successive planes for the $\langle 100 \rangle$ axis. Figure 4 shows the values of L_{v1} in the case of the $\langle 110 \rangle$ axis, calculated across the channel and along the bond, as indicated by the insets. The dotted line corresponds to the average density of valence electrons. The two densities produce quite similar results, except for the midbond region where the solid-state curve exceeds the free-atom values by 25%. Both densities predict a substantial reduction of L_{v1} in the middle of the $\langle 110 \rangle$ channel. In the case of the solid-state density, the minimum value of L_{v1} amounts to 21% of the average value. The results obtained in the case of the $\langle 100 \rangle$ axis are shown in Fig. 5. Let us note that "along bond" means here: along the projection of the bond. The differences between the L_{v1} functions corresponding to the solid-state and free-atom densities are even smaller in this case. Surprisingly, the absolute minimum of L_{v1} across the channel and along the bond is found at a distance of about 0.3 Å from the atom rows and not at the center of the channel. Thus the minimum energy loss observed in the case of the $\langle 100 \rangle$ axial channeling is in fact due to the impact-parameter dependence
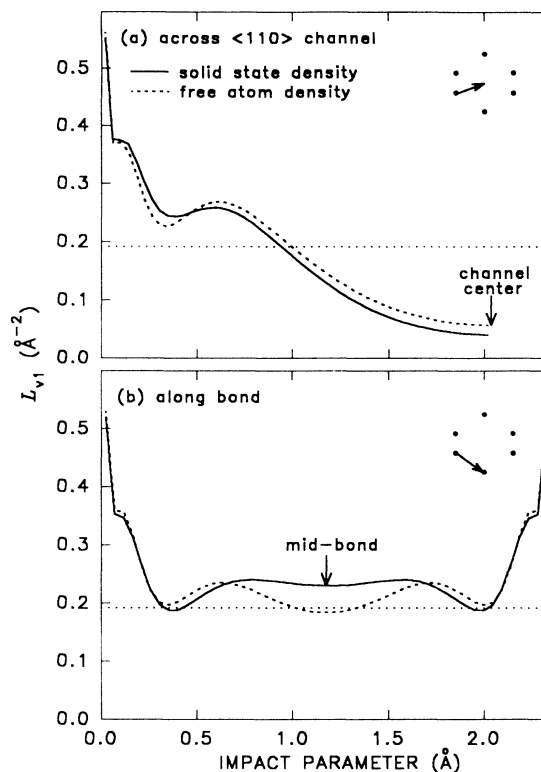
FIG. 4. L_{v1} functions for the solid-state and free-atom valence electron densities for the $\langle 110 \rangle$ axis in Si (a) across the channel and (b) along the bond, as indicated in the insets.
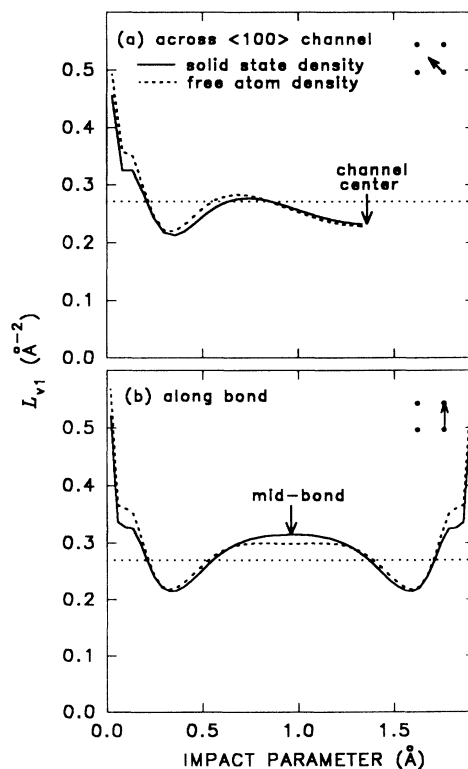
FIG. 5. L_{v1} functions for the solid-state and free-atom valence electron densities for the $\langle 100 \rangle$ axis in Si (a) across the channel and (b) along the projection of the bond, as indicated in the insets.

of the energy loss to core electrons (cf. Fig. 2), which overcompensates the valence electron term shown in Fig. 5.

The above approach to the position-dependent valence electron stopping, which assumes the contribution due to close collisions to be proportional to the local valence electron density, while the contribution due to distant collisions is taken proportional to the average density of valence electrons, will be referred to as the *two-component FEG model*. In addition, to investigate sensitivity of the energy distributions to various assumptions about the valence electron stopping, two limiting cases are considered. First, the nonuniformity of the valence electron gas is disregarded, i.e., the total energy loss to valence electrons is made proportional to their average density. This approach will be referred to as the *constant density model*. Second, the contributions due to both close and distant collisions are assumed to be proportional to the local density of valence electrons. Then the total energy loss to valence electrons is given by $\Delta E_v(\mathbf{b}) = \varepsilon_v L_{v1}(\mathbf{b})$, where $\varepsilon_v = \varepsilon_{v1} + \varepsilon_{v2}$. Based on Eqs. (8) and (9), one obtains

$$\varepsilon_v = \beta \frac{4\pi Z_1^2 e^4}{m_e v^2} Z_v \ln \frac{2m_e v^2}{\hbar \omega_p} . \tag{10}$$

At our projectile velocity ($v/v_F \approx 5$) the above expression agrees to within 0.5% with the results given by Lindhard and Winther [40], if the local value of ω_p is used. Although in our calculations the plasma frequency corresponding to the average valence electron density has been used, it only has a minor effect on the results, as ω_p enters in Eq. (10) through the logarithm. Therefore this approach will be referred to as the *Lindhard-Winther (LW) model*.

IV. RESULTS AND DISCUSSION

A. Energy distributions

Seeking to reproduce the experimental energy distributions, we will use the SCA model to determine the impact-parameter dependence of the energy loss to core electrons. The MEEA model only serves as a simple approximation to the more accurate SCA calculation and will be used later on to test the sensitivity of the energy distributions to the core electron contribution to $\Delta E(b)$. In order to investigate the influence of the valence electron term on the distributions, we first consider the three approaches to the valence electron stopping, discussed in Sec. III B 3. The stopping cross sections due to valence electrons are calculated from Eqs. (8)–(10), assuming $\beta = 1$. For 625-keV H ions in Si one obtains the following values (in eV Å^2): $\varepsilon_{v1} = 42.2$, $\varepsilon_{v2} = 25.3$, and $\varepsilon_v = 67.5$. In order to reproduce the random stopping value of $\varepsilon_r = 108.2$ eV Å^2 [51], one has to assume the core electron term to be $\varepsilon_c = 40.7$ eV Å^2. However, the SCA calculation yields $\varepsilon_c^{\text{SCA}} = 38.4$ eV Å^2. Therefore, in determining losses to core electrons, the impact-parameter dependence given by the L_c function is multiplied by ε_c corresponding to $\beta = 1$. The distributions for the $\langle 110 \rangle$ axial

and the $\{111\}$ planar directions, calculated using (i) the constant density model, (ii) the two-component FEG model, and (iii) the LW model, are compared with the experimental data in Fig. 6 [(ii) and (iii) are with the solid-state valence electron density; see Sec. III B 3]. The constant density model clearly overestimates channeling energy losses, while the LW model gives too large an energy dispersion in the case of the $\langle 110 \rangle$ distribution. The two-component FEG model is seen to reproduce features of the experimental distributions quite well for both the axial and the planar directions. These observations are consistent with a recent analysis of the H ion stopping by valence electrons in Si at lower incident energies of 50–300 keV [35].

The two-component FEG model with the solid-state valence electron density, together with the SCA model, was thus used to calculate the distributions for all directions studied in the $\langle 110 \rangle$ experiment. In order to achieve the best overall agreement β was reduced to 0.94. The simulation results for a set of 12 representative distributions are compared with the experimental data in Fig. 7. When assessing agreement between the simulation and experiment, the low-energy part of the distributions is not taken into account, as it is affected by the overlapping Si signal (cf. Sec. II). The distribution for the $\langle 110 \rangle$ axial direction can still be better reproduced if $\beta = 0.97$ is used. However, the $\langle 110 \rangle$ distribution is
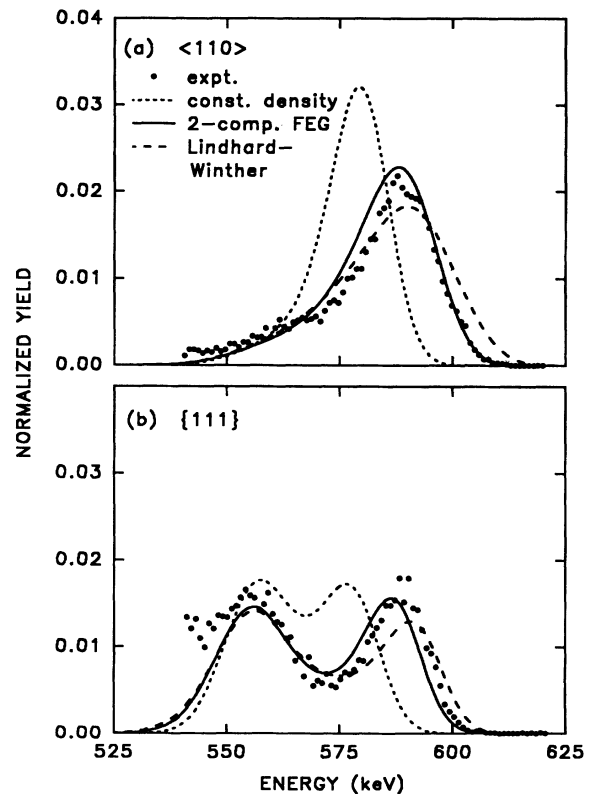
FIG. 6. Energy distributions for (a) the $\langle 110 \rangle$ axial and (b) the $\{111\}$ planar directions, calculated using the SCA model ($\beta = 1$) and (i) the constant density, (ii) the two-component FEG, and (iii) the LW models, compared with experimental data.

most sensitive to crystal imperfections and we prefer to give more weight to the distributions for other directions, in particular the {111} planar direction at $\theta = 10°$.

The present model (with $\beta = 0.94$) was also tested against our previous experiment for the $\langle 100 \rangle$ axis [39]. The distributions simulated for 12 representative directions are compared with the experimental data in Fig. 8. Here the tilt θ is referenced to the $\langle 100 \rangle$ axis and the azimuth ϕ is taken relative to the {110} plane. Unlike the distributions near the $\langle 110 \rangle$ axis, the distributions shown in Fig. 8 do not exhibit well-resolved structures. The reason for this is twofold: first, the ratio of channeled to random energy losses for the $\langle 100 \rangle$ axis is larger than for the $\langle 110 \rangle$ axis (the channel radii for the $\langle 100 \rangle$ and $\langle 110 \rangle$ axes are 1.36 and 2.04 Å, respectively); second, the Si crystal used in the $\langle 100 \rangle$ experiment was half the thickness of the crystal used in the $\langle 110 \rangle$ experiment, which resulted in a poorer *relative* energy resolution in the former case. Nevertheless, the excellent agreement between the simulated and experimental distributions

shown in Fig. 8 gives additional support for the energy-loss model used.

In the calculations above, the influence of surface layers due to C deposition during the measurements was not taken into account, as it had been found negligible in our previous study for the $\langle 100 \rangle$ direction [39]. The distributions near the $\langle 110 \rangle$ direction, however, are more sensitive to any imperfections in the crystal. Therefore, the influence of surface layers was additionally studied in this case. The thickness of the C surface layer for the $\langle 110 \rangle$ measurement was estimated to be 5×10^{15} atoms/cm^2, while in the case of the {111} planar channeling it amounts to about 3×10^{16} atoms/cm^2. The simulations of energy distributions were done for crystals covered with the above C layers as well as a thin silicon oxide layer (3×10^{15} O atoms/cm^2 and 2×10^{15} Si atoms/cm^2). In comparison with the distributions obtained for perfect single crystals (without any surface layers), no significant changes in the shape of the distributions were found. One concludes, therefore, that in the case of the $\langle 110 \rangle$

H beam energy 625 keV, Si crystal thickness 1.2 μm
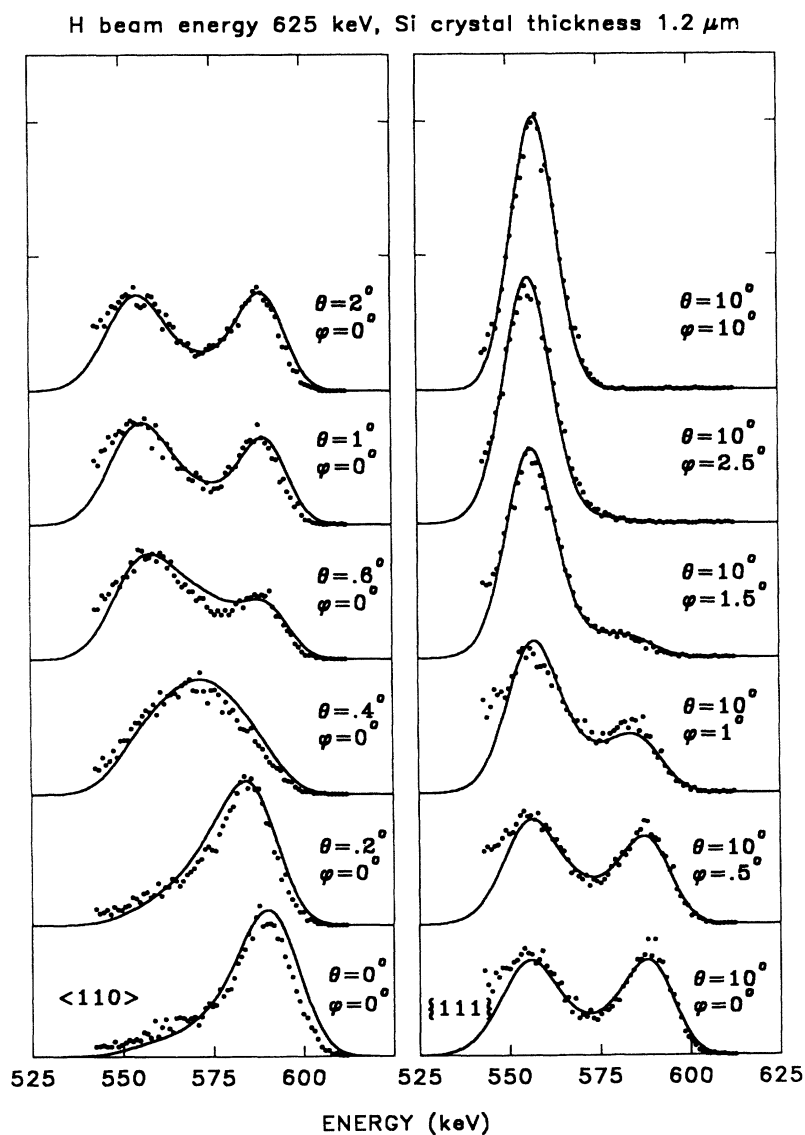
FIG. 7. Monte Carlo simulated energy distributions (solid lines) using the SCA model together with the two-component FEG model with the solid-state valence electron density ($\beta = 0.94$), compared with experimental data (dots) for directions near the $\langle 110 \rangle$ axis.

ENERGY (keV)

experiment, the influence of surface layers on the distributions can also be neglected.

It has been shown earlier in this section that the assumption of a constant valence electron density, as compared to the nonuniform solid-state density, has a marked influence on the distributions. A related question concerns the comparison of the solid-state valence electron density vs the free-atom density. It has often been argued that the inclusion of the solid-state effects in the valence electron density is essential for a quantitative explanation of the stopping of channeled ions. The simulations have been done for the $\langle 110 \rangle$ and $\langle 100 \rangle$ axes and the $\{111\}$ and $\{110\}$ planes using the RHF valence electron density. A comparison with the simulations based on the solid-state density revealed no significant differences in the distributions, as illustrated in the case of the $\langle 110 \rangle$ axial direction in Fig. 9. This can be easily understood if

one refers to Figs. 4 and 5, which present L_{v1} functions for the two electron densities.

The simulations were also done using the MEEA to calculate the energy loss to core electrons (cf. Sec. III B 2). The valence electron contribution to the stopping was evaluated within the two-component FEG model with the solid-state electron density and $\beta = 0.94$. Based on the results presented in Sec. III B 2, the mean excitation energy of 1.4 times the binding energy was used to determine L_c. The energy distributions thus obtained show virtually no difference with respect to the calculation done using the SCA model (Fig. 7). This result confirms that the minor differences between the L_c functions for the two models, displayed in Fig. 3, are of no consequence as far as the energy distributions are concerned. In order to investigate the sensitivity of the distributions to the assumed L_c dependence, two additional simula-

H beam energy 625 keV, Si crystal thickness 0.57 μm
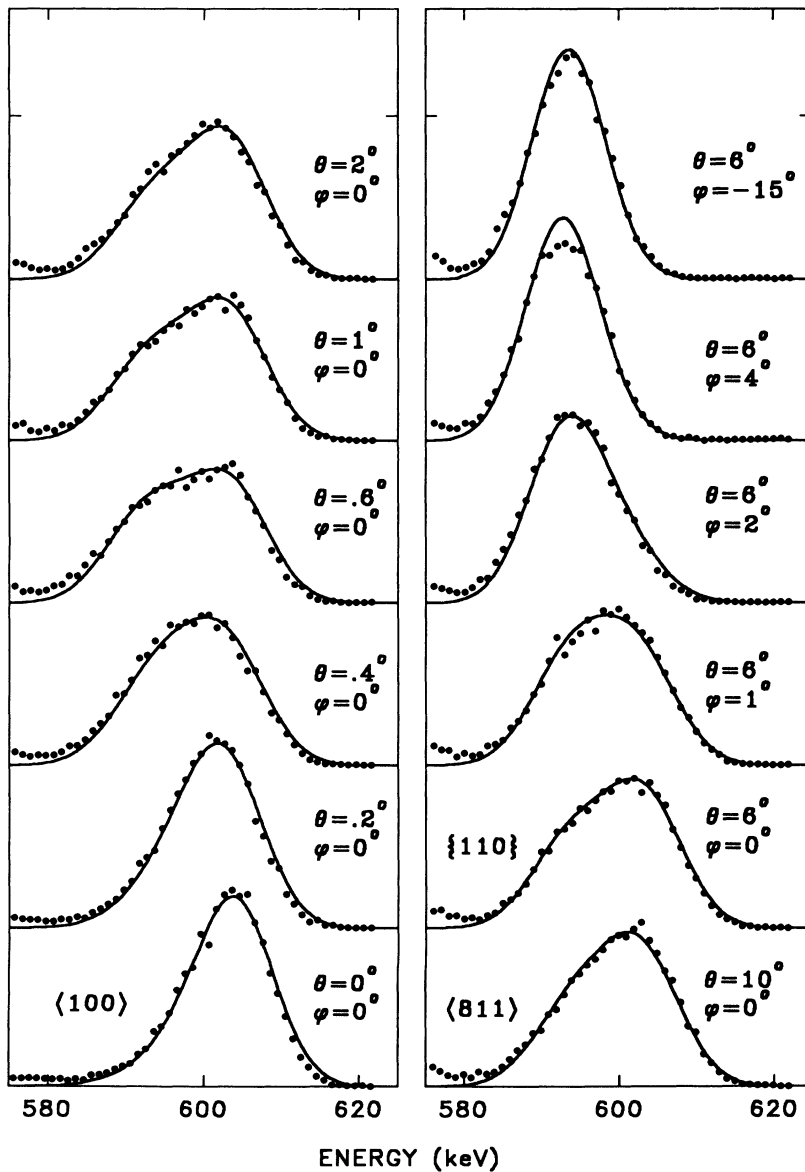
FIG. 8. Monte Carlo simulated energy distributions (solid lines) using the SCA model together with the two-component FEG model with the solid-state valence electron density ($\beta = 0.94$), compared with experimental data (dots) for directions near the $\langle 100 \rangle$ axis.
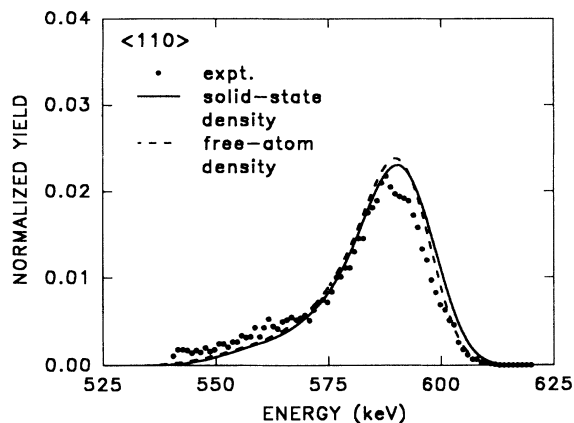
FIG. 9. Energy distributions for the $\langle 110 \rangle$ axial direction calculated using the SCA model together with the two-component FEG model ($\beta = 0.94$) with (i) the solid-state and (ii) the free-atom valence electron densities, compared with experimental data.

tions were done for the MEEA model with $\Omega = 1$ (cf. Fig. 3). These were for the $\langle 110 \rangle$ axis and the $\{111\}$ plane. The results are presented in Fig. 10, in comparison with the SCA distributions and the experimental data. The overestimation of the channeled ion energy losses by the MEEA model with $\Omega = 1$ is clearly seen.
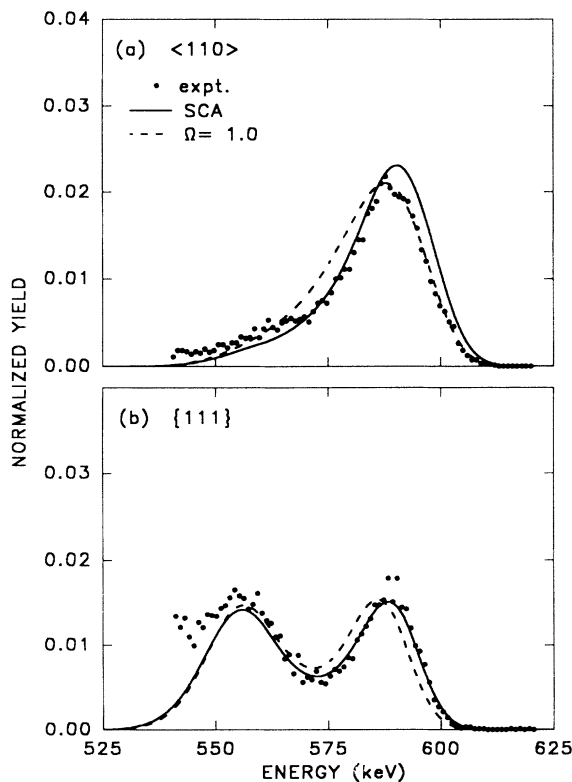
FIG. 10. Energy distributions for (a) the $\langle 110 \rangle$ axial and (b) the $\{111\}$ planar directions, calculated using the two-component FEG model with the solid-state valence electron density ($\beta = 0.94$) together with SCA and MEEA ($\Omega = 1.0$), compared with experimental data.

The results presented in this section show that the experimental distributions near the $\langle 110 \rangle$ and $\langle 100 \rangle$ axes in Si can be very well reproduced by the simulation using the SCA model for core electrons and the two-component FEG model for valence electrons. The stopping cross section for valence electrons, however, has to be reduced by 6% with respect to the values given by Eqs. (8) and (9). Also, an increase of some 10–14 % with respect to the SCA prediction is needed for the energy loss to core electrons. Both the SCA and the FEG theories employed treat the ion stopping within first-order perturbation theory. Estimates of the Barkas effect within the free-electron-gas model [60,61] give in our case about a 1–2 % increase of the stopping due to the Z_1^3 term in the perturbation series. Although the Z_1^4 term is expected to be negative [60,62], it does not seem likely to account for the correction of 6% found in the present work. Similarly, the negative correction for the higher-order terms in the case of the H ion stopping due to core electrons in Si, obtained in Ref. [53], seems to contradict the results of this study.

B. Analysis of ion trajectories

The energy distributions corresponding to the angular scan through the $\langle 110 \rangle$ axis, presented in Fig. 7, change rapidly with the tilt angle. A single-peak distribution for the axial direction shifts towards lower energies and broadens as the tilt increases ($\theta = 0.2°$ and $0.4°$). At a tilt of $0.6°$, splitting of the distribution into two components is first observed. These will be referred to as the channeling and the random components. With a further increase of the tilt, the area of the channeling component increases. The observed evolution corresponds to the transition from axial to planar channeling, which has been a subject of continued interest [63,33,47].

As the experimental distributions are very closely reproduced by the present simulations, it seems worthwhile to examine individual trajectories and the ion flux distribution in order to try to gain a better understanding of the observed axial to planar channeling transition. Figure 11 shows projections of trajectories onto the interaction zone (as used in the simulation code), calculated for four tilts ($0°$, $0.2°$, $0.4°$, and $0.6°$). Atom rows are indicated by black dots. Each trajectory starts in the center of the $\langle 110 \rangle$ channel and is followed to a depth of 1.2 μm. If a trajectory leaves the interaction zone it is put back at an equivalent point. One can see that the trajectories for $\theta = 0°$ and $0.2°$ are very similar. The main difference between them is that the amplitude of the transverse motion in the case of $\theta = 0.2°$ is slightly larger than that for $\theta = 0°$ The trajectory for $\theta = 0.4°$ penetrates almost the whole area of the channel and it still does not display features of the $\{111\}$ planar channeling. The planar channeling is clearly seen, however, in the case of $\theta = 0.6°$.

Although the above observations are based on single trajectories only, they are corroborated by the flux distributions shown for the four directions in Fig. 12. In each case 2000 trajectories were followed to a depth of 0.6 μm. A concentration of the flux in the central region

of the channel diminishes gradually as one goes from $\theta=0°$ to $0.2°$ and on to $0.4°$. At $\theta=0.6°$, a concentration of the flux along the $\{111\}$ planar channel can be seen.

C. Azimuthally averaged mean energy loss near the $\langle 110 \rangle$ axis

In measuring the random energy loss using a single crystal one needs to avoid any channeling effects. This may prove difficult unless one knows precisely the directions that correspond to the so-called random incidence. In order to identify randomlike directions, it is first necessary to know how much tilt away from the axis is needed to avoid any influence of the axis. Once a tilt has been identified as free from axial influence, a detailed study of azimuthal effects (planar channeling) must then be done to fully pinpoint randomlike directions.

The first question can be best addressed by studying the energy loss for the so-called rotating axial dip, i.e., the azimuthally averaged mean energy loss as a function of the tilt angle with respect to the axis. Alternatively, one might look into the (azimuthally averaged) probability of the close encounter processes. This last approach has recently been applied for the $\langle 100 \rangle$ axis in Si [44]. We are not aware, however, of any rotating dip studies for the mean energy loss, which we undertook by the simulation of the energy distributions at a number of tilts from the $\langle 110 \rangle$ axis $(0° < \theta < 16°$, with a step of $0.25°)$, using the four-component model of Ref. [39] (version C). At each tilt, 64 000 trajectories were followed to a depth of 0.5 μm. The azimuthal averaging was accomplished by randomly selecting the azimuthal angle ϕ for each incident ion within the interval $[0°, 360°)$, assuming uniform probability distribution. The resulting mean energy losses, normalized to the random energy loss, are presented in Fig. 13. The statistical uncertainty of the points shown is less than 0.2%. Although the values shown depart from the random level by a fraction of a percent
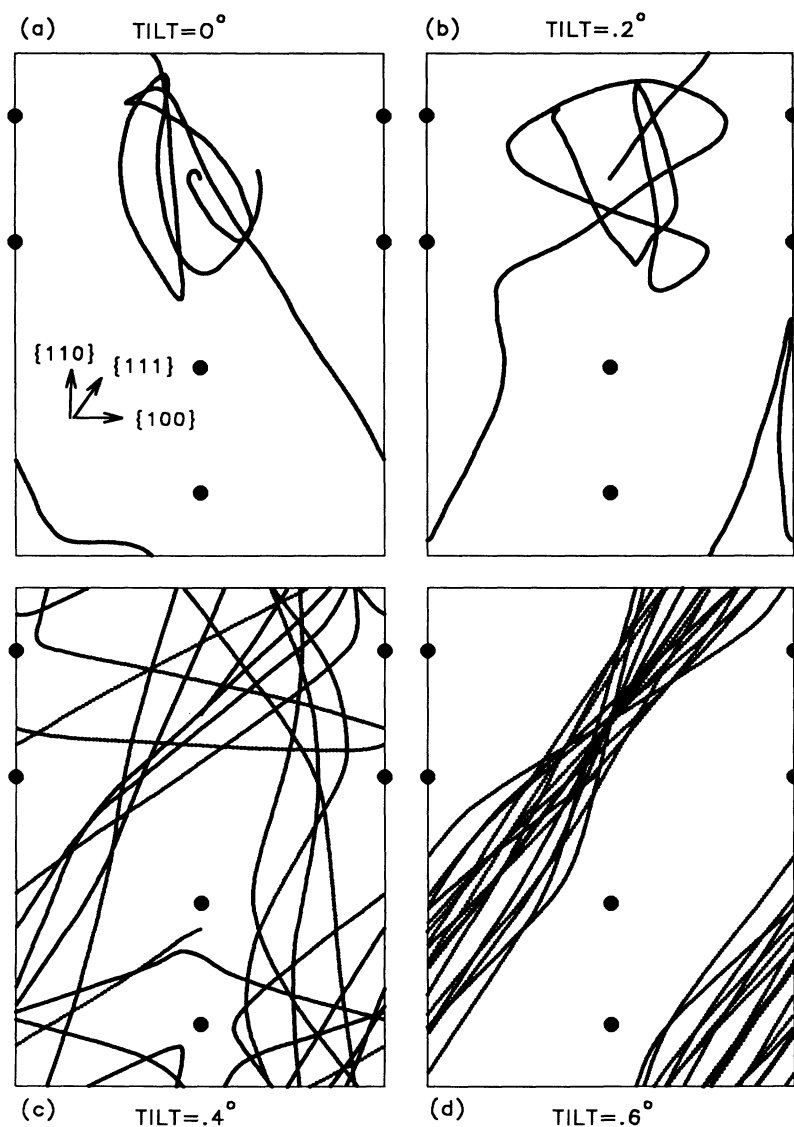
FIG. 11. Projections of trajectories onto the interaction zone calculated for four tilts (a) $0°$, (b) $0.2°$, (c) $0.4°$, and (d) $0.6°$ for the $\langle 110 \rangle$ axis. Black dots indicate atom rows.

(a)   TILT = 0°

(b)   TILT = .2°

(c)   TILT = .4°

(d)   TILT = .6°
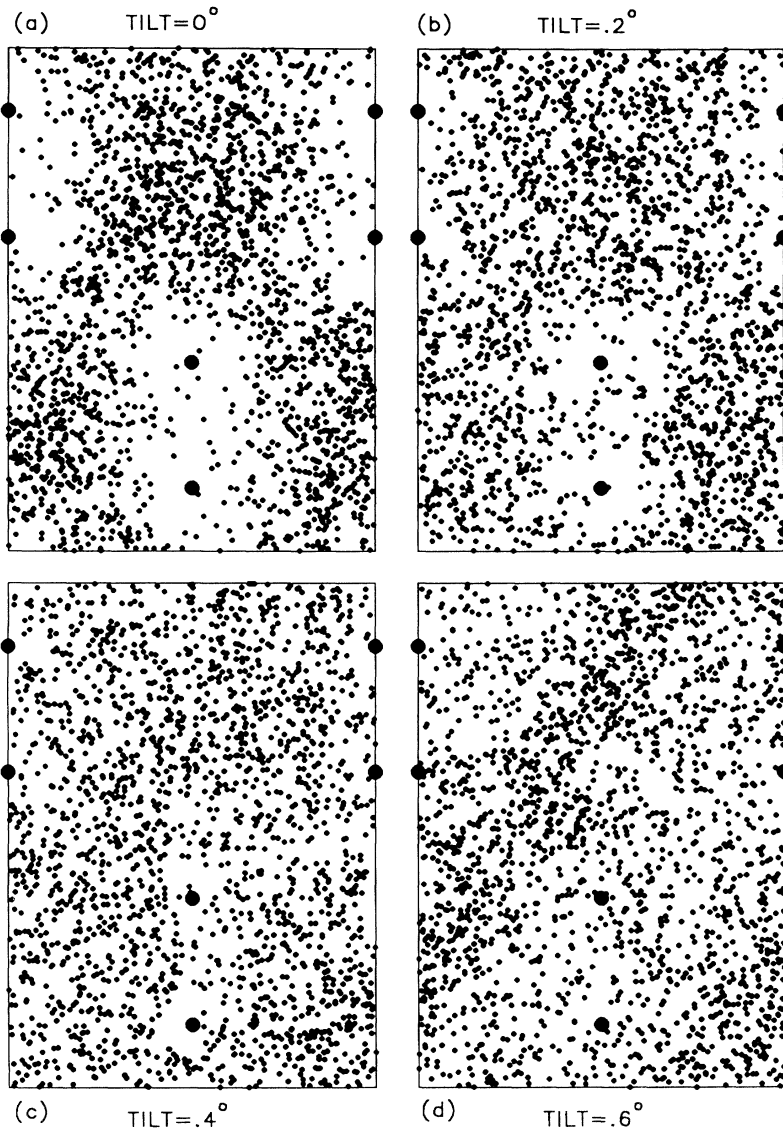
FIG. 12. Ion flux distributions for four tilts (a) 0°, (b) 0.2°, (c) 0.4°, and (d) 0.6° from the $\langle 110 \rangle$ axis.

only, the shoulder of the $\langle 110 \rangle$ axial dip can be seen, as well as a fine structure for tilts $\theta > 10°$. One concludes that the influence of the $\langle 110 \rangle$ dip extends until tilts exceed $\theta \approx 9°$. In accord with Ref. [44], the observed fine structure can be explained by the influence of planar channels tangential to the azimuthal scans at certain tilts. In the present case $\{123\}$, $\{158\}$, and $\{135\}$ planes were identified by means of the stereographic projection shown in Fig. 14.

Finally, a detailed azimuthal scan (for the mean energy loss) was calculated for the tilt of 10° used in the experiment. The results presented in Fig. 15 display a number of low- as well as high-index planar dips. Additionally, energy losses increased by up to 5% over the random value are observed over substantial intervals of the azimuthal angle. The energy loss for the randomlike direction used in the $\langle 110 \rangle$ experiment, namely, tilted by 10° off the axis and azimuthally rotated by 10° with respect to the $\{111\}$ plane (towards the nearest $\{100\}$ plane), is seen to differ by less than 1% from the random value.
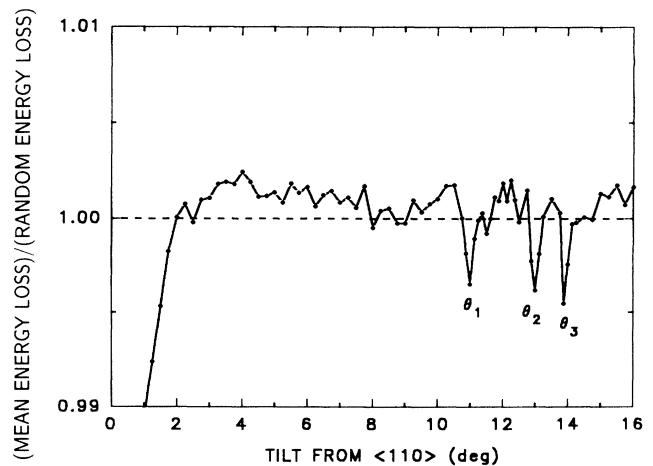
FIG. 13. Azimuthally averaged mean energy loss (relative to the random energy loss) as a function of tilt from the $\langle 110 \rangle$ axis.
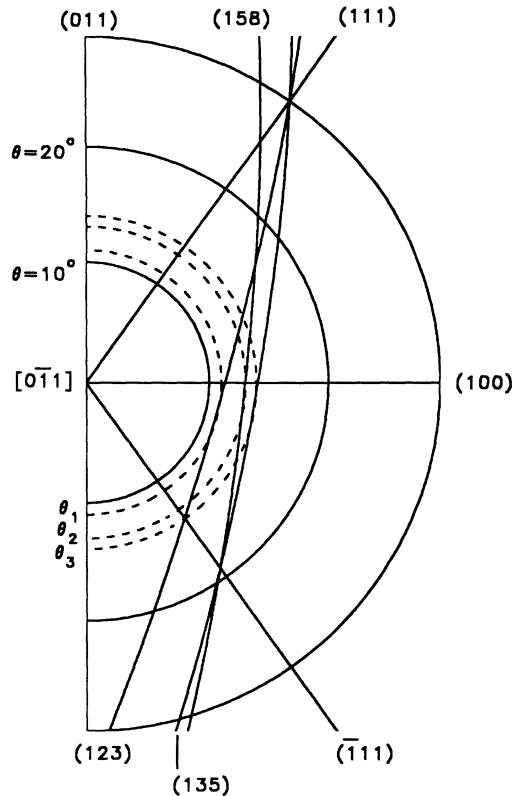
FIG. 14. Stereographic projection for the [0$\bar{1}$1] axis, showing various planes [(123), (158), and (135)] running tangent to the azimuthal scans for tilts θ_1, θ_2, and θ_3 (cf. Fig. 13).

FIG. 15. Mean energy loss (relative to the random energy loss) for an azimuthal scan taken at a tilt of 10° from the ⟨110⟩ axis.

V. CONCLUSIONS

Based on the comparison between experimental and Monte Carlo simulated energy-loss distributions for 625-keV H$^+$ ions transmitted through thin Si single crystals, it has been found that the impact-parameter dependence of the ion energy loss can be well described by the SCA model applied to core electrons and the two-component FEG model applied to valence electrons. These models, based on first-order perturbation theory, reproduce very closely the extensive set of experimental distributions corresponding to detailed angular scans through axial and planar channels in Si, if a small adjustment of the stopping cross sections due to core and valence electrons is made. The corrections found, however, do not appear to be consistent with the current estimates of the contribu-

tion to the stopping due to the higher-order terms in the perturbation series.

The dependence of the energy loss to core electrons on the impact parameter, predicted by the SCA model, can be surprisingly well approximated by the MEEA model with the parameter $\Omega = 1.4$. Therefore, at least in distant collisions of the ion with core electrons, the mean excitation energy is about 1.4 times greater than the binding energy for a given shell. It has also been found that the local-density approximation of Lindhard and Winther applied to valence electrons does not agree with the experimental data as well as the two-component FEG model does. The comparison between the solid-state and free-atom valence electron densities has shown a rather unexpected insensitivity of the energy distributions to the solid-state effects in the electron density in Si.

ACKNOWLEDGMENTS

[1] Channeling: Theory, Observation, and Applications, edited by D. V. Morgan (Wiley, New York, 1973).

[2] D. S. Gemmell, Rev. Mod. Phys. 46, 129 (1974).

[3] L. C. Feldman, J. W. Mayer, and S. T. Picraux, Materials Analysis by Ion Channeling (Academic, New York, 1982).

[4] M. A. Kumakhov and F. F. Komarov, Energy Loss and Ion Ranges in Solids (Gordon and Breach, New York, 1981).

[5] A. R. Sattler and G. Dearnaley, Phys. Rev. Lett. 15, 59 (1965); Phys. Rev. 161, 244 (1967).

[6] B. R. Appleton, C. Erginsoy, and W. M. Gibson, Phys. Rev. 161, 330 (1967).

[7] G. Della Mea, A. V. Drigo, S. Lo Russo, P. Mazzoldi, and G. G. Bentini, Radiat. Eff. 13, 115 (1972).

[8] F. H. Eisen and J. Bøttiger, in Atomic Collisions in Solids, edited by S. Datz, B. R. Appleton, and C. D. Moak (Ple-

num, New York, 1975), Vol. 2, p. 919.

[9] J. D. Melvin and T. A. Tombrello, Radiat. Eff. **26**, 113 (1975).

[10] F. Cembali and F. Zignani, Radiat. Eff. **31**, 169 (1977).

[11] A. Carnera, G. Della Mea, A. V. Drigo, S. Lo Russo, P. Mazzoldi, and G. G. Bentini, Phys. Rev. B **17**, 3492 (1978).

[12] P. Gehrmann, K. Lenkeit, and R. Stolle, Phys. Status Solidi B **131**, 519 (1985).

[13] J. Lindhard, K. Dan. Vidensk. Selsk. Mat. Fys. Medd. **34**, No. 14 (1965).

[14] M. Kitagawa and Y. H. Ohtsuki, Phys. Rev. B **5**, 3418 (1972).

[15] K. Dettmann and M. T. Robinson, Phys. Rev. B **10**, 1 (1974).

[16] F. F. Komarov and M. A. Kumakhov, Radiat. Eff. **22**, 1 (1974).

[17] K. Dettmann, Z. Phys. A **272**, 227 (1975).

[18] A. Desalvo and R. Rosa, J. Phys. C **10**, 1595 (1977).

[19] V. V. Beloshitsky and M. A. Kumakhov, Radiat. Eff. **35**, 209 (1978).

[20] H. Esbensen and J. A. Golovchenko, Nucl. Phys. A **298**, 382 (1978).

[21] A. F. Burenkov, F. F. Komarov, and M. A. Kumakhov, Phys. Status Solidi B **99**, 417 (1980).

[22] O. H. Crawford and C. W. Nestor, Phys. Rev. A **28**, 1260 (1983).

[23] E. Kührt and R. Wedell, Phys. Status Solidi B **116**, 585 (1983).

[24] V. A. Khodyrev and E. I. Sirotinin, Phys. Status Solidi B **116**, 659 (1983).

[25] A. Grass-Marti, Nucl. Instrum. Methods B **9**, 1 (1985).

[26] H. Ascolani and H. A. Arista, Phys. Rev. A **33**, 2352 (1986).

[27] E. C. Goldberg and V. H. Ponce, Radiat. Eff. **100**, 139 (1986).

[28] N. M. Kabachnik, V. N. Kondratev, and O. V. Chumanova, Phys. Status Solidi B **145**, 103 (1988).

[29] S. Namiki, H. Nitta, and Y. H. Ohtsuki, Phys. Rev. B **37**, 1448 (1988).

[30] E. H. Mortensen, H. H. Mikkelsen, and P. Sigmund, Nucl. Instrum. Methods B **61**, 139 (1991).

[31] L. R. Logan, C. S. Murthy, and G. R. Srinivasan, Phys. Rev. A **46**, 5754 (1992).

[32] S. Steenstrup and A. P. Pathak, Radiat. Eff. **55**, 17 (1981).

[33] G. Della Mea, A. V. Drigo, S. Lo Russo, P. Mazzoldi, G. G. Bentini, A. Desalvo, and R. Rosa, Phys. Rev. B **7**, 4029 (1973).

[34] A. Dygo and A. Turos, Phys. Lett. A **127**, 281 (1988).

[35] K. Lenkeit, Ch. Trikalinos, L. L. Balashova, N. M. Kabachnik, and V. I. Shulga, Phys. Status Solidi B **161**, 513 (1990).

[36] Ch. Trikalinos, L. L. Balashova, N. M. Kabachnik, and V. I. Shulga, Nucl. Instrum. Methods B **69**, 94 (1992).

[37] C. S. Murthy and G. R. Srinivasan, Phys. Rev. B **47**, 1256 (1993).

[38] P. W. L. van Dijk, L. J. van IJzendoorn, M. de Koning, P.

Bobbert, W. van Haeringen, and M. J. A. de Voigt, Nucl. Instrum. Methods B **85**, 551 (1994).

[39] A. Dygo, M. A. Boshart, M. W. Grant, and L. E. Seiberling, Nucl. Instrum. Methods B **93**, 117 (1994).

[40] J. Lindhard and A. Winther, K. Dan. Vidensk. Selsk. Mat. Fys. Medd. **34**, No. 4 (1964).

[41] L. E. Seiberling, P. F. Lyman, and M. W. Grant, J. Vac. Sci. Technol. A **11**, 715 (1993).

[42] A. Dygo, W. N. Lennard, and I. V. Mitchell, Nucl. Instrum. Methods B **74**, 581 (1993).

[43] A. Dygo and A. Turos, Phys. Rev. B **40**, 7704 (1989).

[44] A. Dygo, W. N. Lennard, I. V. Mitchell, and P. J. M. Smulders, Nucl. Instrum. Methods B **84**, 23 (1994); **90**, 161 (1994).

[45] A. Dygo and A. Turos, Nucl. Instrum. Methods B **48**, 219 (1990).

[46] A. Dygo, P. J. M. Smulders, and D. O. Boerma, Nucl. Instrum. Methods B **64**, 701 (1992).

[47] P. J. M. Smulders, A. Dygo, and D. O. Boerma, Nucl. Instrum. Methods B **67**, 185 (1992).

[48] A. Dygo, W. N. Lennard, and I. V. Mitchell, Nucl. Instrum. Methods B **90**, 142 (1994).

[49] J. F. Ziegler, J. P. Biersack, and U. Littmark, *The Stopping and Range of Ions in Solids* (Pergamon, New York, 1985).

[50] Q. Yang and D. J. O'Connor, Nucl. Instrum. Methods B **61**, 149 (1991).

[51] J. F. Ziegler and H. H. Andersen, *Hydrogen Stopping Powers and Ranges in All Elements* (Pergamon, New York, 1977).

[52] L. L. Balashova, V. Ya. Chumanov, O. V. Chumanova, G. A. Iferov, A. F. Tulinov, N. M. Kabachnik, and V. N. Kondratev, Nucl. Instrum. Methods B **33**, 168 (1988); N. M. Kabachnik, *ibid.* **69**, 76 (1992).

[53] L. L. Balashova, T. V. Grankina, N. M. Kabachnik, and G. P. Pokhil, Nucl. Instrum. Methods B **48**, 156 (1990); L. L. Balashova, N. M. Kabachnik, and V. N. Kondratev, Phys. Status Solidi B **161**, 113 (1990).

[54] C. Auth and H. Winter, Phys. Lett. A **176**, 109 (1993).

[55] N. M. Kabachnik, O. V. Chumanova, and V. Ya. Chumanov, Nucl. Instrum. Methods B **83**, 591 (1993).

[56] E. Clementi and C. Roetti, At. Data Nucl. Data Tables **14**, 177 (1974).

[57] *CRC Handbook of Chemistry and Physics*, edited by D. R. Lide (CRC, Boca Raton, FL, 1992).

[58] The branch for $b < 0.46$ Å was calculated using the parameters $c_0 = 1.1847$, $c_1 = 0$, $c_2 = 0.2220$, and $c_3 = -6.8265$.

[59] M. Deutsch, Phys. Rev. B **45**, 646 (1992).

[60] J. Lindhard, Nucl. Instrum. Methods **132**, 1 (1976).

[61] C. C. Sung and R. H. Ritchie, Phys. Rev. A **28**, 674 (1983).

[62] H. H. Mikkelsen, Nucl. Instrum. Methods B **58**, 136 (1991).

[63] B. R. Appleton, J. H. Barrett, T. S. Noggle, and C. D. Moak, Radiat. Eff. **13**, 171 (1972); B. R. Appleton, C. D. Moak, T. S. Noggle, and J. H. Barrett, Phys. Rev. Lett. **28**, 1307 (1972).